# Numerical and Experimental Investigation of the Near Wake Dynamics for a Square Prism

J-D. Kim[1], B. Havel[2], H. Hangan* [1,2]

[1]*Boundary Layer Wind Tunnel Laboratory*
[2]*Advanced Fluid Mechanics Group*
*University of Western Ontario, London, Ontario, Canada*

## Abstract

The shear layer formation and the near wake regions of a square prism are numerically (LES) and experimentally (LDV) investigated. The time averaged and phase averaged velocity field is analyzed. It is found that the vortex dynamics in the near wake is similar to the models proposed by Perry and co-workers for different bluff bodies. New inside into the vortex dynamics of the two regions is obtained by analyzing the phase averaged streamlines for both regions.

## 1 Introduction

In one of the first investigations of the near-wake flow region Perry et al. (1982) have used flow visualizations for a circular cylinder and based on instantaneous streamlines inferred the essential topology for this laminar case. For turbulent flows Cantwell & Coles (1983) and Perry and Steiner have used 'flying-wire' techniques to characterize the near-wake region of a circular cylinder and of flat plates, respectively. Rodi et al (1993) have used phase averaged unidirectional LDV measurements to investigate the shear layer formation zone on the lateral surface of a square prism. Previous numerical (both RANS and LES) work did not yet investigate the macro-structure dynamics of this region (Murakami et al. 1995).

Herein both the shear layer formation and the near turbulent wake regions of a square prism are investigated using a combination of LES and two-dimensional phase-averaged LDV measurements in an attempt to understand the relation between these two flow regions in relation to vortex shedding.

The time-averaged and phase averaged flow field on the lateral surface of the prism are firstly investigated in a manner similar to Rodi et al. The LES and experimental (LDV) results are compared for this flow region to assess differences and to gain confidence in the numerical approach. The LES generated topology of the phase-averaged velocity field both the shear layer

* Corresponding author, E-mail : hmh@blwtl.uwo.ca

formation and the near-wake regions is afterwards analysed. A vortex shedding formation process similar to the one inferred by Perry et al (1982) is observed in the near wake region. Finally the near wake and the shear layer formation zones are related and some particular vortex dynamics aspects are presented. Numerical and Experimental Set-up and Results

## 2. Numerical and Experimental Set-up and Results

### 2.1 Numerical set-up

A grid filter operation of characteristic length $\Delta$ is applied to the continuity and unsteady incompressible Navier-Stokes equations.
The filtered Navier-Stokes equations with a standard Smagorinski's model are :

$$\dot{\bar{u}}_i + (\bar{u}_i \bar{u}_j)_{,j} = -\left(\bar{p} + \frac{2}{3} k_{SGS}\right)_{,i} + \left(\frac{1}{\mathrm{Re}} + \nu_{eff}\right)\left(\bar{u}_{i,j} + \bar{u}_{j,i}\right)_{,j}$$

In order to take into account the near wall effect, $\Delta$ is multiplied by the Van Driest type wall damping function.
The finite volume method and a MAC type coupling algorithm are employed. Central difference method is used in space with a semi-implicit time marching scheme. The 2nd order Adams-Bashforth method for convection terms and the 2nd order Crank-Nicolson method for the diffusion terms are used.

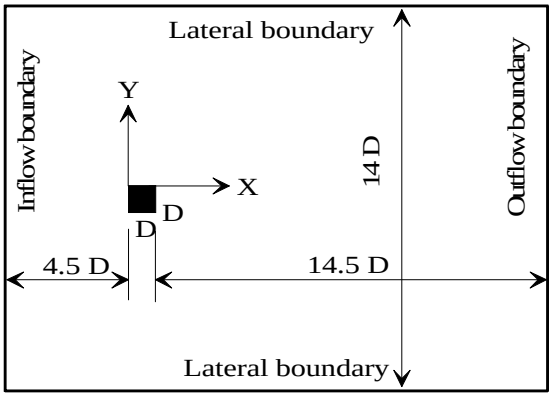


Fig. 1 Computational domain

The choice of boundary conditions is as follows: no-slip condition for the cylinder surface; constant velocity at the inlet and convection condition for the

* Corresponding author, E-mail : hmh@blwtl.uwo.ca

outlet; periodic conditions in the spanwise direction and symmetry conditions along the lateral direction.
Fig. 1 shows the computational domain which dimensions are 20D in streamwise direction, 14D in lateral direction, and 2D in spanwise direction. A total of 107120 ($N_x$*$N_y$*$N_z$ = 104*103*10) computational cells are used at the current preliminary calculation. The smallest cell is 2% of D, where D is a dimension of the square cylinder section.
The linear system of equations for pressure is solved using an Incomplete Cholesky Conjugate Gradient (ICCG) method. The calculations are carried out on a Cray SV1 vector supercomputers. The hyperplane approach to vectorize the ICCG solver was used(Van der Vorst, 1989). The code executed at a speed of 240 Mflops on a single CPU.

### 2.2 Experimental set-up

The experiments were carried out in a suction-type open wind tunnel of cross-section 46 cm x 46 cm with an oncoming streamwise turbulence intensity of less than 1.5 %. The square cylinder spanned the entire cross-section and had made a blockage of 6.5 %. The Reynolds number based on cylinder dimension, oncoming free-stream velocity was 22,000 in air.

Simultaneous two-component Laser-Doppler Anemometer measurements were taken in backward-scatter mode with an optical probe of 453 mm focal length. The frequency shift was varied between 1 and 10 MHz to allow the recording of the turbulent velocity events within filter settings. Seeding of the flow field was accomplished using 1:10 glycerol-water mixture, atomized at a number mean diameter of 4 microns.

At each point 60,000 velocity events were recorded in parallel with the pressure time trace on the centre of the cylinder. A peak detection algorithm was employed on the pressure signal to define the periods for the phase-averaging. Each period was resolved into 20 phase angles.

## 3 Results

### 3.1 Velocity and Reynolds Stresses in the Shear-layer Formation Zone

Similar to Lyn and Rodi (1994), the phase averaged (symbols) and time averaged (continuous lines) streamwise velocity profiles at the top sidewall of the square prism at various x/d positions are plotted in Fig. 2. Both the experimental and the LES results show the deviation of the phase-averages from the time average increasing downstream with maximum differences between the accelerating (phase 5) and decelerating (phase 15) phases of phase 1. Deviations

* Corresponding author, E-mail : hmh@blwtl.uwo.ca

are larger for the shear layer zone compared to the free-stream in accordance with Lyn and Rodi's results. LES fails to reproduce the 'jet-nose' acceleration phase (phase 5) behavior which has been previously observed by Lyn and Rodi and is observed herein in the LDV data. This is attributed to the coarser numerical grid.

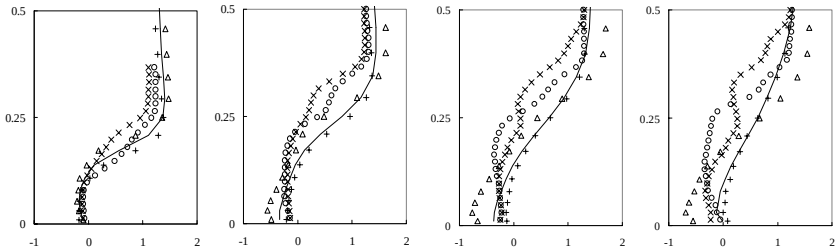

(a) (b) (c) (d)

Fig. 2 Time averaged and phase averaged velocity profiles at (a) x/D=0.25, (b) x/D=0.50, (c) x/D=0.75, (d) x/D=1.0 ( + phase 05(LES), Δ phase 15(LES), —— mean(LES), x phase 05(EXP), o phase 15(EXP))

Fig. 3 shows the deviations between the time averaged and phase averaged streamwise Reynolds stress profiles for LES only. These results compare well with Lyn and Rodi's experiment showing similar shapes and magnitudes as well as vertical positions of maxima. The vertical oscillation of the shear layer (the distance between the accelerating and decelerating phases maxima) is less for LES as compared to experiments.

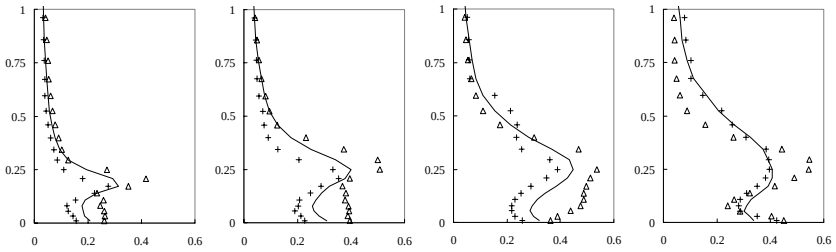

(a) (b) (c) (d)

Fig. 3 Turbulent Reynolds normal stress profiles ,<u'> at (a) x/D=0.25, (b) x/D=0.50, (c) x/D=0.75, (d) x/D=1.0

Fig. 4 presents the LES acceleration (phase 5) and deceleration (phase 15) cross-stream normal Reynolds stresses. The movement of the peaks as well as the changes in phase magnitude can be related to the phase averaged sectional streamlines in Fig. 7a, phases 5 and 15. The maximum difference between the two phases corresponds to the midpoint position (x/d=0.5) for which phase 5 corresponds to the centre of the recirculation vortex and phase 15 is shifted streamwise and upwards. The shear Reynolds stresses are shown in Fig. 5. and

* Corresponding author, E-mail : hmh@blwtl.uwo.ca

they exquibit the largest magnitudes and deviation between the acceleration/deceleration phases towards the upstream corner in the production dominated flow zones. The profiles of the streamwise velocity gradients are presented in Fig. 6 and they show a strong correlation with the streamwise normal stresses, Fig. 4 with similar magnitudes, and behaviour as in the experiment of Lyn and Rodi.

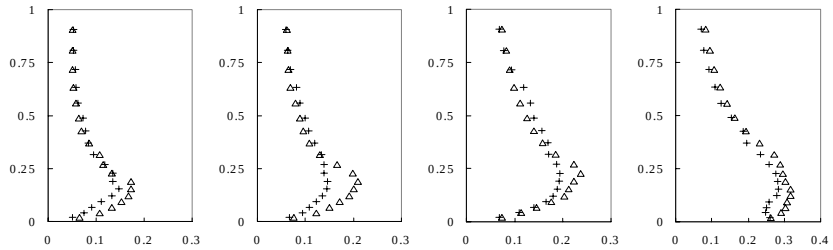

(a) (b) (c) (d)

Fig. 4 Turbulent Reynolds normal stress profiles, <v'> at (a)x/D=0.25, (b) x/D=0.50, (c) x/D=0.75, (d) x/D=1.0

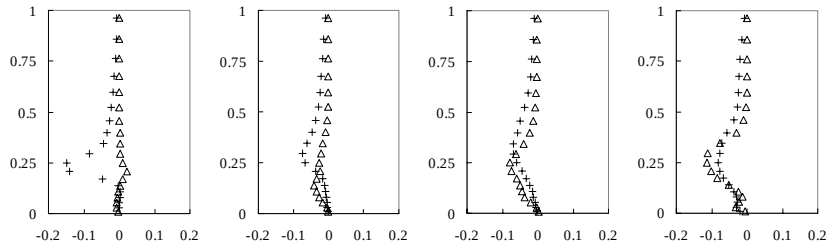

(a) (b) (c) (d)

Fig. 5 Turbulent Reynolds stress profiles ,<u'v'> at (a) x/D=0.25, (b) x/D=0.50, (c) x/D=0.75, (d) x/D=0.989

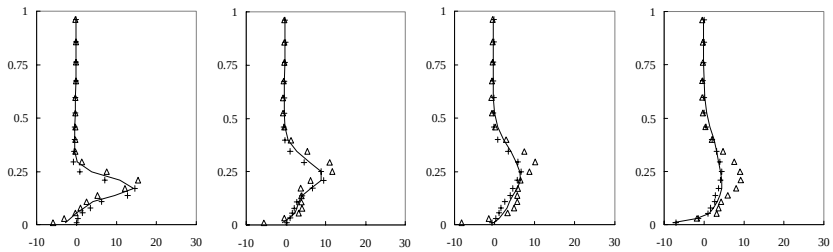

(a) (b) (c) (d)

Fig. 6 Time averaged and phase averaged du/dy profiles at (a) x/D=0.25, (b) x/D=0.50, (c) x/D=0.75, (d) x/D=1.0

* Corresponding author, E-mail : hmh@blwtl.uwo.ca

## 3.2 Streamlines

Time averaged sectional streamlines on the sidewall are presented in Fig. 7a and b for LES and the present LDV experiments, respectively. The main three features: the main recirculation vortex, the saddle point and the secondary vortex are present in both the experiments and the LES. However the LES recirculation is centred lower at y/D =0.15 as compared to the experiments(y/D=0.2) in association with a lower position of the saddle point as well.

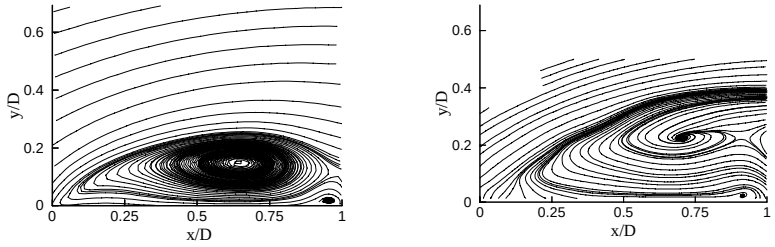


(a) (b)

Fig. 7 Time averaged streamlines, (a) Large eddy simulation, (b) Experiment

The phase-averaged sectional streamlines for LES and experiments are presented in Fig. 8. The LES reveal both the shear layer formation and the near wake region while the experiments show only the sidewall formation zone. Firstly the two sets of results compare very well and this aspect enhances the confidence level to the LES results. Both data sets have been phase-averaged similarly using the centre sidewall pressure information as trigger.

Perry et al (1982) have put forward a laminar flow vortex shedding model that later Perry and Steiner (1987) have shown it may be applied for turbulent flow as well. The nature of the bluff bodies studied by Perry and collaborators (circular cylinders and flat plates) cannot provide an insight into the relation between the near wake vortex shedding mechanism and the separation and shear layer formation zone on the sidewall of the body.

Herein, Fig. 8a allows us for the first time to relate the two flow areas in an attempt of better understanding the vortex formation mechanics. If we look exclusively at the near wake (base) region Fig. 8a shows a vortex shedding mechanism very similar to the one put forward by Perry and al. (1982). The starting phase 1 can be considered as the phase at which the shedding happens being charaterised by a main saddle point S. Looking forward from phase 5 we observe the formation of a clockwise vortex at the downstream corner which vortex grows until phase 11 when a symmetric situation to phase 1 is expected and shedding occurs again. The interesting mechanism is the formation and growing of the counterclockwise trailing vortex in phase 17 continuing growing until the shedding occurs back in phase 1. The dynamics of this vortex can be related to the formation of the secondary saddle point S' in phase 1, Fig. 9, in addition to the classical (Perry like) main saddle S. The existence of two saddle points together with the two secondary vortices C1 and C2 at the trailing edge

* Corresponding author, E-mail : hmh@blwtl.uwo.ca

are particular to the square prism case characterized by an interaction between the two flow zones: shear layer formation and the near wake. It is interesting that immediately after the shedding phase 1 the two vortices (C1 and C2) disappear. Further analysis is needed to decide if they cancel out or they merge with the adjacent von Karman vortices.

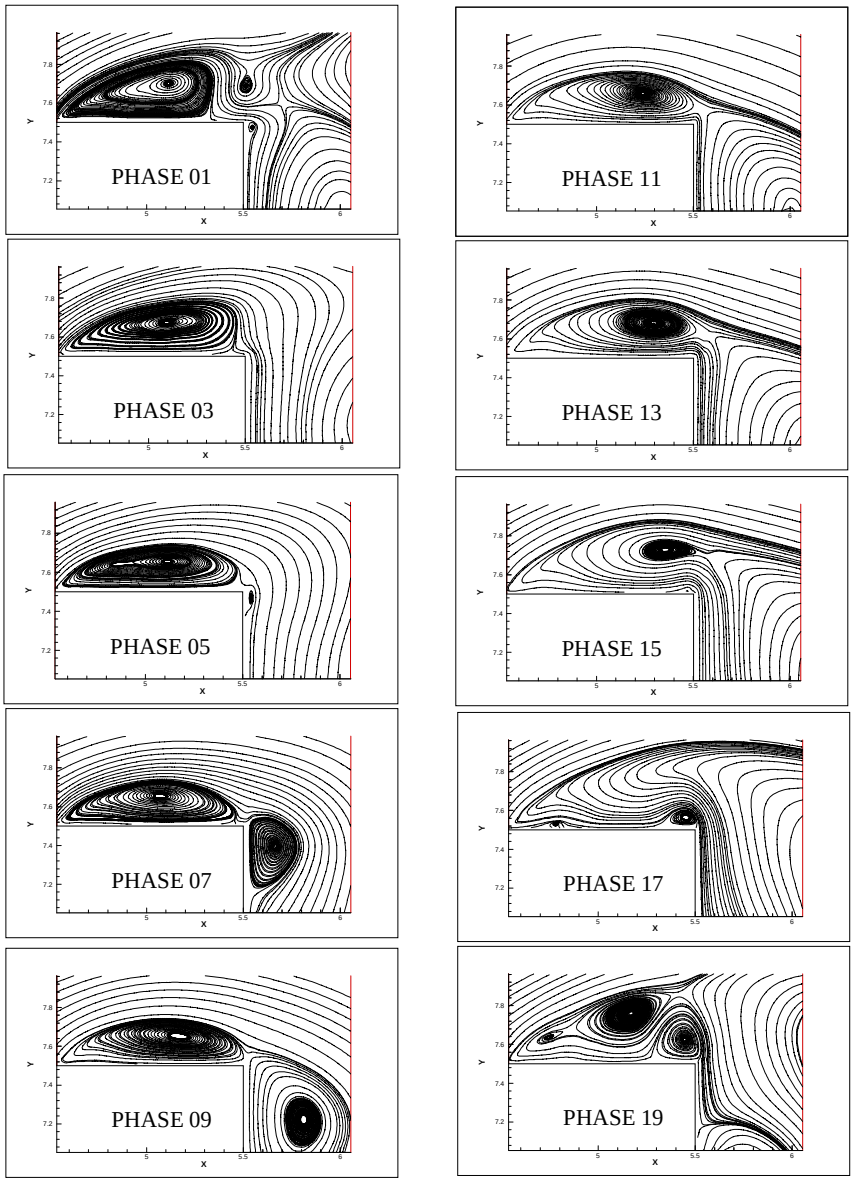


Fig. 8 a Phase averaged streamlines (LES)

* Corresponding author, E-mail : hmh@blwtl.uwo.ca

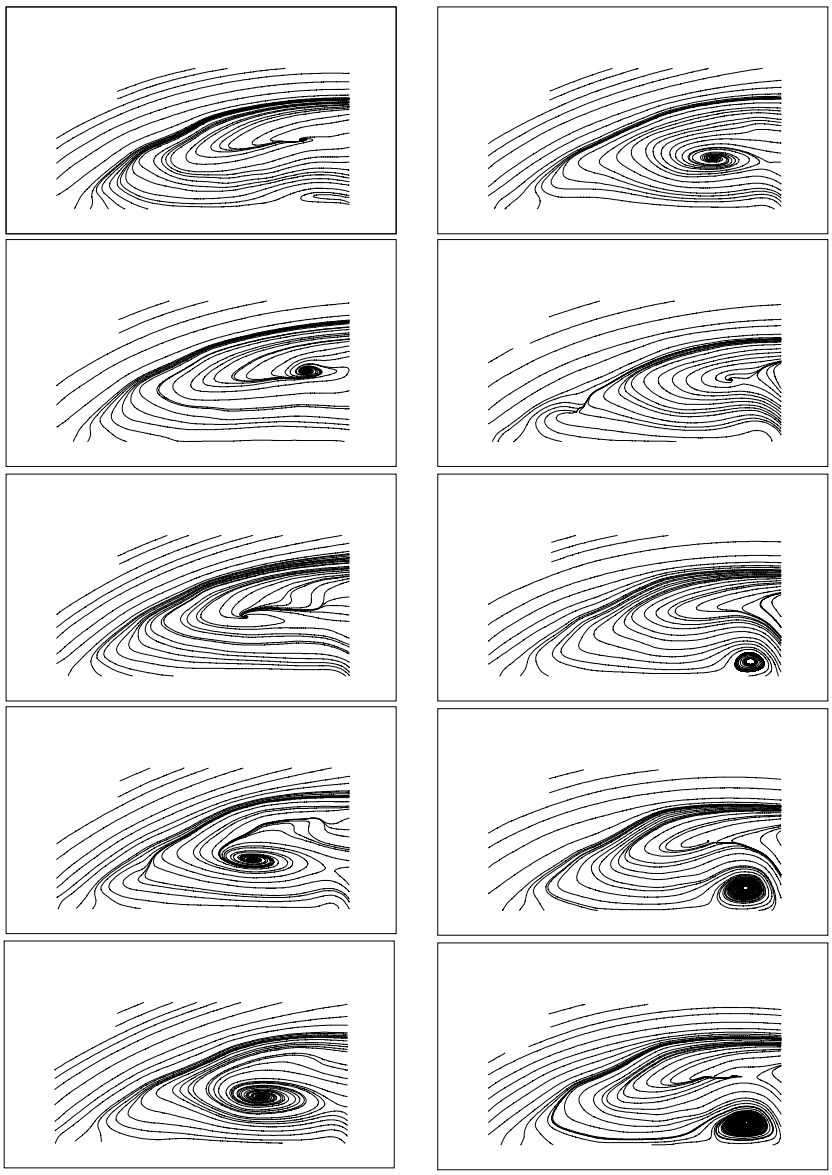

Fig. 8 b Phase averaged streamlines (Experiment)

* Corresponding author, E-mail : hmh@blwtl.uwo.ca

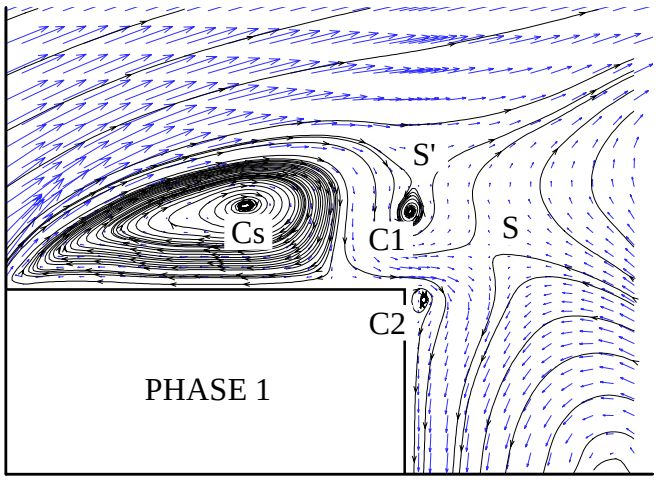


Fig. 9 Phase 1, Vortex shedding

## 4 Conclusions

The near wake and the shear layer formation flows for a square prism are investigated in an attempt to relate the vortex dynamics in the two regions. LES and LDV results are compared for the sidewall (shear formation) region and satisfactory agreement is found.
The LES results are then used to expand into phase average investigation of both flow regions. It is found that the near wake region dynamics is similar to the models proposed by Perry and co-workers. Finally the interrelation between the vortex dynamics in the two regions is analysed and secondary vortex and saddle points are identified and discussed.

## References

B.J. Cantwell and D. Coles, An experimental study of entrainment and transport in the turbulent near wake of a circular cylinder, J. Fluid Mech. (1983), vol. 136, pp. 321-374

D.A. Lyn, S.Einav, W.Rodi and J.H.Park, " A laser-Doppler velocimetry study of ensemble-averaged characteristics of the turbulent near wake of a square cylinder" J. Fluid Mech. 304 (1995), 285-319

* Corresponding author, E-mail : hmh@blwtl.uwo.ca

D.A. Lyn, W.Rodi "The flapping shear layer formed by flow separation from the forward corner of a square cylinder" J. Fluid Mech. 267 (1994), 353-376

S. Murakami, A. Mochida, "On turbulent vortex shedding flow past 2D square cylinder predicted by CFD" J. Wind Eng. and Ind. Aerodynamics 54 (1995) 191-211

A.E. Perry, M.S. Chong and T.T. Lim, The vortex-shedding process behind two-dimensional bluff bodies, J. Fluid Mech. (1982), vol. 116, pp. 77-90

A.E. Perry, T.R. Steiner, Large-scale vortex structures in turbulent wakes behind bluff bodies. Part 1. Vortex formation processes, J. Fluid Mech. (1987), vol. 174, pp. 233-270

H.A. Van der Vorst, ICCG and related methods for problems on vector computers. Computer Physics Communications, 53 (1989) 223-235

H. Werner, H. Wengle (1991) Large-eddy simulation of turbulent flow over and around a cube in a plate channel, Turbulent Shear Flows 8, Springer-Verlag

* Corresponding author, E-mail : hmh@blwtl.uwo.ca